

Box 8.3 | Volcanic Eruptions as Analogues

Volcanic eruptions provide a natural experiment of a stratospheric aerosol cloud that can serve to inform us of the impacts of the proposed production of such a cloud as a means to control the climate, which is one method of geoengineering (Rasch et al., 2008); see Section 7.7. For example, Trenberth and Dai (2007) showed that the Asian and African summer monsoon, as well as the global hydrological cycle, was weaker for the year following the 1991 Mt Pinatubo eruption, which is consistent with climate model simulations (Robock et al., 2008). MacMynowski et al. (2011) showed that because the climate system response of the hydrological cycle is rapid, forcing from volcanic eruptions, which typically last about a year, can serve as good analogues for longer-lived forcing. The formation of sulphate aerosols, their transport and removal, their impacts on ozone chemistry, their RF, and the impacts on whitening skies all also serve as good analogues for geoengineering proposals. Volcanic impacts on the carbon cycle because of more diffuse radiation (Mercado et al., 2009) and on remote sensing can also be useful analogues, and the impacts of contrail-generated sub-visual cirrus (Long et al., 2009) can be used to test the long-term impacts of a permanent stratospheric cloud.

Smoke from fires generated by nuclear explosions on cities and industrial areas, which could be lofted into the stratosphere, would cause surface cooling and a reduction of stratospheric ozone (Mills et al., 2008). Volcanic eruptions that produce substantial stratospheric aerosol clouds also serve as an analogue that supports climate model simulations of the transport and removal of stratospheric aerosols, their impacts on ozone chemistry, their RF, and the climate response. The use of the current global nuclear arsenal still has the potential to produce nuclear winter, with continental temperatures below freezing in summer (Robock et al., 2007a; Toon et al., 2008), and the use of only 100 nuclear weapons could produce climate change unprecedented in recorded human history (Robock et al., 2007b), with significant impacts on global agriculture (Özdoğan et al., 2013; Xia and Robock, 2013).

8.4.2.3 Records of Past Volcanism and Effects of Very Large Eruptions

Although the effects of volcanic eruptions on climate are largest in the 2 years following a large stratospheric injection, and the winter warming effect in the NH has been supported by long-term records (Fischer et al., 2007), there is new work indicating extended volcanic impacts via long-term memory in the ocean heat content and sea level (Stenchikov et al., 2009; Gregory, 2010; Otterå et al., 2010). Zanchettin et al. (2012) found changes in the North Atlantic Ocean circulation that imply strengthened northward oceanic heat transport a decade after major eruptions, which contributes to the emergence of extensive winter warming over the continental NH along with persistent cooling over Arctic regions on decadal time scales, in agreement with Zhong et al. (2011) and Miller et al. (2012).

New work on the mechanisms by which a supereruption (Self and Blake, 2008) could force climate has focused on the 74,000 BP eruption of the Toba volcano (2.5°N, 99.0°E). Robock et al. (2009) used simulations of up to 900 times the 1991 Mt Pinatubo sulphate injection to show that the forcing is weaker than that predicted based on a linear relationship with the sulphate aerosol injection. The results agreed with a previous simulation by Jones et al. (2005). They also showed that chemical interactions with ozone had small impacts on the forcing and that the idea of Bekki et al. (1996) that water vapour would limit and prolong the growth of aerosols was not supported. Timmreck et al. (2010) however, incorporating the idea of Pinto et al. (1989) that aerosols would grow and therefore both have less RF per unit mass and fall out of the atmosphere more quickly, found much less of a radiative impact from such a large stratospheric input.

8.4.2.4 Future Effects

We expect large eruptions over the next century but cannot predict when. Ammann and Naveau (2003) and Stothers (2007) suggested an 80-year periodicity in past eruptions, but the data record is quite short and imperfect, and there is no mechanism proposed that would cause this. While the period 1912–1963 was unusual for the past 500 years in having no large volcanic eruptions, and the period 1250–1300 had the most globally climatically significant eruptions in the past 1500 years (Gao et al., 2008), current knowledge only allows us to predict such periods on a statistical basis, assuming that the recent past distributions are stationary. Ammann and Naveau (2003), Gusev (2008), and Deligne et al. (2010) studied these statistical properties and Ammann and Naveau (2010) showed how they could be used to produce a statistical distribution for future simulations. Although the future forcing from volcanic eruptions will depend only on the stratospheric aerosol loading for most forcing mechanisms, the future effects on reducing ozone will diminish as ozone-depleting substances diminish in the future (Eyring et al., 2010b).

8.5 Synthesis of Global Mean Radiative Forcing, Past and Future

The RF can be used to quantify the various agents that drive climate change over the Industrial Era or the various contributions to future climate change. There are multiple ways in which RF can be attributed to underlying causes, each providing various perspectives on the importance of the different factors driving climate change. This section evaluates the RF with respect to emitted component and with respect to the ultimate atmospheric concentrations. The uncertainties in the RF

agents vary and the confidence levels for these are presented in this section. Finally, this section shows historical and scenarios of future time evolution of RF.

8.5.1 Summary of Radiative Forcing by Species and Uncertainties

Table 8.5 has an overview of the RF agents considered here and each of them is given a confidence level for the change in RF over the Industrial Era to the present day. The confidence level is based on the evidence (robust, medium, and limited) and the agreement (high, medium, and low; see further description in Chapter 1). The confidence level of the forcing agents goes beyond the numerical values available in estimates and is an assessment for a particular forcing agent to have a real

value within the estimated range. Some of the RF agents have robust evidence such as WMGHG with well documented increases based on high precision measurements as well as contrails as additional clouds which can be seen by direct observations. However, for some forcing agents the evidence is more limited regarding their existence such as aerosol influence on cloud cover. The consistency in the findings for a particular forcing agent determines the evaluation of the evidence. A combination of different methods, for example, observations and modeling, and thus the understanding of the processes causing the forcing is important for this evaluation. The agreement is a qualitative judgment of the difference between the various estimates for a particular RF agent. Figure 1.11 shows how the combined evidence and agreement results in five levels for the confidence level.

Table 8.5 | Confidence level for the forcing estimate associated with each forcing agent for the 1750–2011 period. The confidence level is based on the evidence and the agreement as given in the table. The basis for the confidence level and change since AR4 is provided. See Figure 1.11 for further description of the evidence, agreement and confidence level. The colours are adopted based on the evidence and agreement shown in Figure 1.11. Dark green is “High agreement and Robust evidence”, light green is either “High agreement and Medium evidence” or “Medium agreement and Robust evidence”, yellow is either “High agreement and limited evidence” or “Medium agreement and Medium evidence” or “Low agreement and Robust evidence”, orange is either “Medium agreement and Limited evidence” or “Low agreement and Medium evidence” and finally red is “Low agreement and Limited evidence”. Note, that the confidence levels given in Table 8.5 are for 2011 relative to 1750 and for some of the agents the confidence level may be different for certain portions of the Industrial Era.

	Evidence	Agreement	Confidence Level	Basis for Uncertainty Estimates (more certain / less certain)	Change in Understanding Since AR4
Well-mixed greenhouse gases	Robust	High	Very high	Measured trends from different observed data sets and differences between radiative transfer models	No major change
Tropospheric ozone	Robust	Medium	High	Observed trends of ozone in the troposphere and model results for the industrial era/Differences between model estimates of RF	No major change
Stratospheric ozone	Robust	Medium	High	Observed trends in stratospheric and total ozone and modelling of ozone depletion/Differences between estimates of RF	No major change
Stratospheric water vapour from CH ₄	Robust	Low	Medium	Similarities in results of independent methods to estimate the RF/Known uncertainty in RF calculations	Elevated owing to more studies
Aerosol–radiation interactions	Robust	Medium	High	A large set of observations and converging independent estimates of RF/Differences between model estimates of RF	Elevated owing to more robust estimates from independent methods
Aerosol–cloud interactions	Medium	Low	Low	Variety of different observational evidence and modelling activities/Spread in model estimates of ERF and differences between observations and model results	ERF in AR5 has a similar confidence level to RF in AR4
Rapid adjustment aerosol–radiation interactions	Medium	Low	Low	Observational evidence combined with results from different types of models/Large spread in model estimates	Elevated owing to increased evidence
Total aerosol effect	Medium	Medium	Medium	A large set of observations and model results, independent methods to derive ERF estimates/Aerosol–cloud interaction processes and anthropogenic fraction of CCN still fairly uncertain	Not provided previously
Surface albedo (land use)	Robust	Medium	High	Estimates of deforestation for agricultural purposes and well known physical processes/Spread in model estimates of RF	Elevated owing to the availability of high-quality satellite data
Surface albedo (BC aerosol on snow and ice)	Medium	Low	Low	Observations of snow samples and the link between BC content in snow and albedo/Large spread in model estimates of RF	No major change
Contrails	Robust	Low	Medium	Contrails observations, large number of model estimates/Spread in model estimates of RF and uncertainties in contrail optical properties	Elevated owing to more studies
Contrail-induced cirrus	Medium	Low	Low	Observations of a few events of contrail induced cirrus/Extent of events uncertain and large spread in estimates of ERF	Elevated owing to additional studies increasing the evidence
Solar irradiance	Medium	Medium	Medium	Satellite information over recent decades and small uncertainty in radiative transfer calculations/Large relative spread in reconstructions based on proxy data	Elevated owing to better agreement of a weak RF
Volcanic aerosol	Robust	Medium	High	Observations of recent volcanic eruptions/Reconstructions of past eruptions	Elevated owing to improved understanding

Notes:

The confidence level for aerosol–cloud interactions includes rapid adjustments (which include what was previously denoted as cloud lifetime effect or second indirect aerosol effect). The separate confidence level for the rapid adjustment for aerosol–cloud interactions is very low. For aerosol–radiation interaction the table provides separate confidence levels for RF due to aerosol–radiation interaction and rapid adjustment associated with aerosol–radiation interaction.

Evidence is robust for several of the RF agents because of long term observations of trends over the industrial era and well defined links between atmospheric or land surfaced changes and their radiative effects. Evidence is medium for a few agents where the anthropogenic changes or the link between the forcing agent and its radiative effect are less certain. Medium evidence can be assigned in cases where observations or modelling provide a diversity of information and thus not a consistent picture for a given forcing agent. We assess the evidence to be limited only for rapid adjustment associated with aerosol–cloud interaction where model studies in some cases indicate changes but direct observations of cloud alterations are scarce. High agreement is given only for the WMGHG where the relative uncertainties in the RF estimates are much smaller than for the other RF agents. Low agreement can either be due to large diversity in estimates of the magnitude of the forcing or from the fact that the method to estimate the forcing has a large uncertainty. Stratospheric water vapour is an example of the latter with modest difference in the few available estimates but a known large uncertainty in the radiative transfer calculations (see further description in Section 8.3.1).

used instead of confidence level. For comparison with previous IPCC assessments the LOSU is converted approximately to confidence level. Note that LOSU and confidence level use different terms for their rankings. The figure shows generally increasing confidence levels but also that more RF mechanisms have been included over time. The confidence levels for the RF due to aerosol–radiation interactions, surface albedo due to land use and volcanic aerosols have been raised and are now at the same ranking as those for change in stratospheric and tropospheric ozone. This is due to an increased understanding of key parameters and their uncertainties for the elevated RF agents. For tropospheric and stratospheric ozone changes, research has shown further complexities with changes primarily influencing the troposphere or the stratosphere being linked to some extent (see Section 8.3.3). The rapid adjustment associated with aerosol–cloud interactions is given the *confidence* level *very low* and had a similar level in AR4. For rapid adjustment associated with aerosol–radiation interactions (previously denoted as semi-direct effect) the *confidence* level is *low* and is raised compared to AR4, as the evidence is improved and is now *medium* (see Section 7.5.2).

Figure 8.14 shows the development of the confidence level over the last four IPCC assessments for the various RF mechanisms. In the previous IPCC reports level of scientific understanding (LOSU) has been

Table 8.6 shows the best estimate of the RF and ERF (for AR5 only) for the various RF agents from the various IPCC assessments. The RF due to WMGHG has increased by 16% and 8% since TAR and AR4,

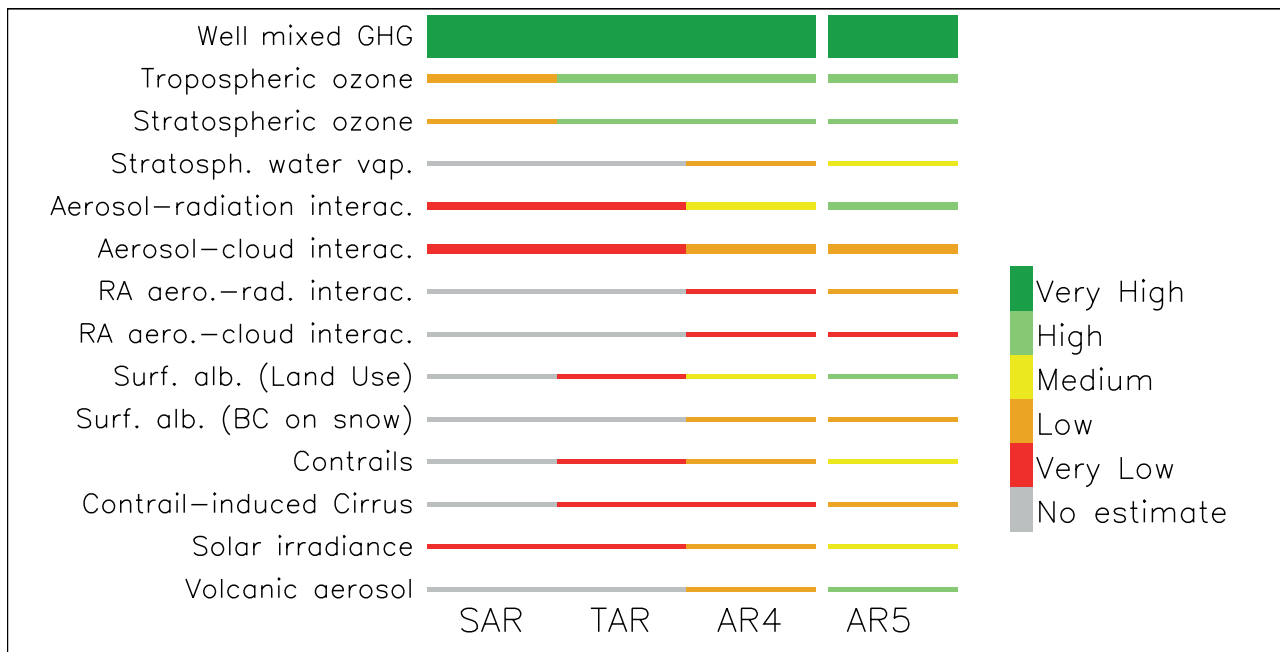


Figure 8.14 | Confidence level of the forcing mechanisms in the 4 last IPCC assessments. In the previous IPCC assessments the level of scientific understanding (LOSU) has been adopted instead of confidence level, but for comparison with previous IPCC assessments the LOSU is converted approximately to confidence level. The thickness of the bars represents the relative magnitude of the current forcing (with a minimum value for clarity of presentation). LOSU for the RF mechanisms was not available in the first IPCC Assessment (Houghton et al., 1990). Rapid adjustments associated with aerosol–cloud interactions (shown as RA aero.–cloud interac.) which include what was previously referred to as the second indirect aerosol effect or cloud lifetime effect whereas rapid adjustments associated with aerosol–radiation interactions (shown as RA aero.–rad. interac.) were previously referred to as the semi-direct effect (see Figure 7.3). In AR4 the confidence level for aerosol–cloud interaction was given both for RF due to aerosol–cloud interaction and rapid adjustment associated with aerosol–cloud interaction. Generally the aerosol–cloud interaction is not separated into various components in AR5, hence the confidence levels for ERF due to aerosol–cloud interaction in AR5 and for RF due to aerosol–cloud interaction from previous IPCC reports are compared. The confidence level for the rapid adjustment associated with aerosol–cloud interaction is comparable for AR4 and AR5. The colours are adopted based on the evidence and agreement shown in Figure 1.11. Dark green is “High agreement and Robust evidence”, light green is either “High agreement and Medium evidence” or “Medium agreement and Robust evidence”, yellow is either “High agreement and limited evidence” or “Medium agreement and Medium evidence” or “Low agreement and Robust evidence”, orange is either “Medium agreement and Limited evidence” or “Low agreement and Medium evidence” and finally red is “Low agreement and Limited evidence”.

respectively. This is due mainly to increased concentrations (see Section 8.3.2), whereas the other changes for the anthropogenic RF agents compared to AR4 are due to re-evaluations and in some cases from improved understanding. An increased number of studies, additional observational data and better agreement between models and observations can be the causes for such re-evaluations. The best estimates for RF due to aerosol–radiation interactions, BC on snow and solar irradiance are all substantially decreased in magnitude compared to AR4; otherwise the modifications to the best estimates are rather small. For the RF due to aerosol–radiation interaction and BC on snow the changes in the estimates are based on additional new studies since AR4 (see Section 8.3.4 and Section 7.5). For the change in the estimate of the solar irradiance it is a combination on how the RF is calculated, new evidence showing some larger earlier estimates were incorrect, and a downward trend observed during recent years in the solar activity that has been taken into account (see Section 8.4.1). The estimate for ERF due to aerosol–cloud interaction includes rapid adjustment but still this ERF is smaller in magnitude than the AR4 RF estimate due to aerosol–cloud interactions without rapid adjustments (a theoretical construct not quantified in AR5). The uncertainties for ERF due to CO₂ increase when compared to RF (see Section 8.3.2). We assume the relative ERF uncertainties for CO₂ apply to all WMGHG. For the short-lived GHG we do not have sufficient information to include separate ERF uncertainty to each of these forcing agents (see Section 8.1.1.3).

However, for these forcing mechanisms the RF uncertainties are larger than for the WMGHG and thus it is *unlikely* that rapid adjustments change the uncertainties substantially.

Figure 8.15 shows the RF for agents listed in Table 8.6 over the 1750–2011 period. The methods for calculation of forcing estimates are described in Section 8.3 and 8.4. For some of the components the forcing estimates are based on observed abundance whereas some are estimated from a combination of model simulations and observations and for others are purely model based. Solid bars are given for ERF, whereas RF values are given as (additional) hatched bars. Similarly the uncertainties are given for ERF in solid lines and dotted lines for RF. An important assumption is that different forcing mechanisms can be treated additively to calculate the total forcing (see Boucher and Haywood, 2001; Forster et al., 2007; Haywood and Schulz, 2007). Total ERF over the Industrial Era calculated from Monte Carlo simulations are shown in Figure 8.16, with a best estimate of 2.29 W m⁻². For each of the forcing agents a probability density function (PDF) is generated based on uncertainties provided in Table 8.6. The combination of the individual RF agents to derive total forcing follows the same approach as in AR4 (Forster et al., 2007) which is based on the method in Boucher and Haywood (2001). The PDF of the GHGs (sum of WMGHG, ozone and stratospheric water vapour) has a more narrow shape than the PDF for the aerosols owing to the much lower relative uncertainty.

Table 8.6 | Summary table of RF estimates for AR5 and comparison with the three previous IPCC assessment reports. ERF values for AR5 are included. For AR5 the values are given for the period 1750–2011, whereas earlier final years have been adopted in the previous IPCC assessment reports.

	Global Mean Radiative Forcing (W m ⁻²)				Comment	ERF (W m ⁻²)
	SAR (1750–1993)	TAR (1750–1998)	AR4 (1750–2005)	AR5 (1750–2011)		AR5
Well-mixed greenhouse gases (CO ₂ , CH ₄ , N ₂ O, and halocarbons)	2.45 (2.08 to 2.82)	2.43 (2.19 to 2.67)	2.63 (2.37 to 2.89)	2.83 (2.54 to 3.12)	Change due to increase in concentrations	2.83 (2.26 to 3.40)
Tropospheric ozone	+0.40 (0.20 to 0.60)	+0.35 (0.20 to 0.50)	+0.35 (0.25 to 0.65)	+0.40 (0.20 to 0.60)	Slightly modified estimate	
Stratospheric ozone	-0.1 (-0.2 to -0.05)	-0.15 (-0.25 to -0.05)	-0.05 (-0.15 to +0.05)	-0.05 (-0.15 to +0.05)	Estimate unchanged	
Stratospheric water vapour from CH ₄	Not estimated	+0.01 to +0.03	+0.07 (+0.02, +0.12)	+0.07 (+0.02 to +0.12)	Estimate unchanged	
Aerosol–radiation interactions	Not estimated	Not estimated	-0.50 (-0.90 to -0.10)	-0.35 (-0.85 to +0.15)	Re-evaluated to be smaller in magnitude	-0.45 (-0.95 to +0.05)
Aerosol–cloud interactions	0 to -1.5 (sulphate only)	0 to -2.0 (all aerosols)	-0.70 (-1.80 to -0.30) (all aerosols)	Not estimated	Replaced by ERF and re-evaluated to be smaller in magnitude	-0.45 (-1.2 to 0.0)
Surface albedo (land use)	Not estimated	-0.20 (-0.40 to 0.0)	-0.20 (-0.40 to 0.0)	-0.15 (-0.25 to -0.05)	Re-evaluated to be slightly smaller in magnitude	
Surface albedo (black carbon aerosol on snow and ice)	Not estimated	Not estimated	+0.10 (0.0 to +0.20)	+0.04 (+0.02 to +0.09)	Re-evaluated to be weaker	
Contrails	Not estimated	+0.02 (+0.006 to +0.07)	+0.01 (+0.003 to +0.03)	+0.01 (+0.005 to +0.03)	No major change	
Combined contrails and contrail-induced cirrus	Not estimated	0 to +0.04	Not estimated	Not estimated		0.05 (0.02 to 0.15)
Total anthropogenic	Not estimated	Not estimated	1.6 (0.6 to 2.4)	Not estimated	Stronger positive due to changes in various forcing agents	2.3 (1.1 to 3.3)
Solar irradiance	+0.30 (+0.10 to +0.50)	+0.30 (+0.10 to +0.50)	+0.12 (+0.06 to +0.30)	+0.05 (0.0 to +0.10)	Re-evaluated to be weaker	

Notes:

Volcanic RF is not added to the table due to the periodic nature of volcanic eruptions, which makes it difficult to compare to the other forcing mechanisms.

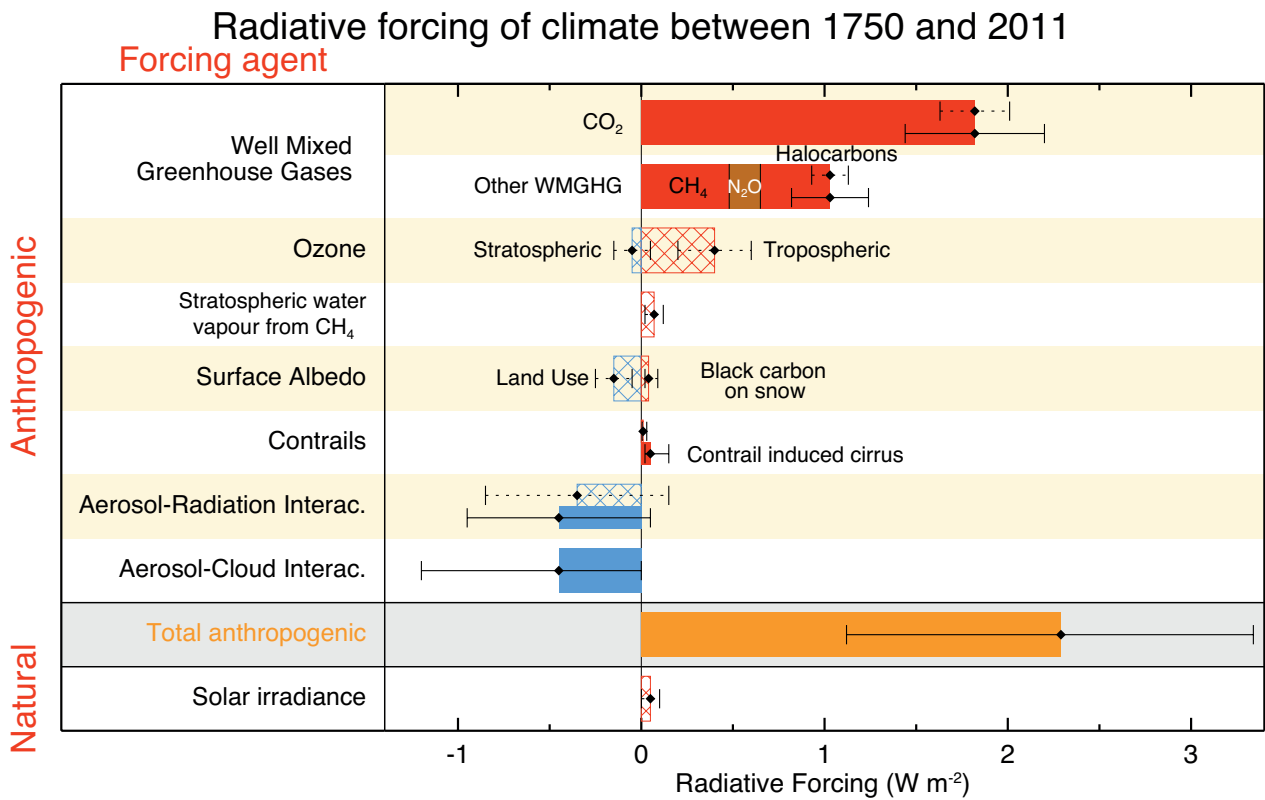


Figure 8.15 | Bar chart for RF (hatched) and ERF (solid) for the period 1750–2011, where the total ERF is derived from Figure 8.16. Uncertainties (5 to 95% confidence range) are given for RF (dotted lines) and ERF (solid lines).

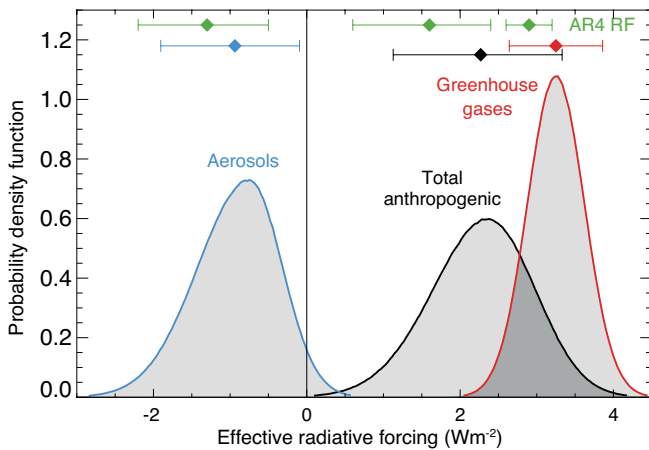


Figure 8.16 | Probability density function (PDF) of ERF due to total GHG, aerosol forcing and total anthropogenic forcing. The GHG consists of WMGHG, ozone and stratospheric water vapour. The PDFs are generated based on uncertainties provided in Table 8.6. The combination of the individual RF agents to derive total forcing over the Industrial Era are done by Monte Carlo simulations and based on the method in Boucher and Haywood (2001). PDF of the ERF from surface albedo changes and combined contrails and contrail-induced cirrus are included in the total anthropogenic forcing, but not shown as a separate PDF. We currently do not have ERF estimates for some forcing mechanisms: ozone, land use, solar, etc. For these forcings we assume that the RF is representative of the ERF and for the ERF uncertainty an additional uncertainty of 17% has been included in quadrature to the RF uncertainty. See Supplementary Material Section 8.SM.7 and Table 8.SM.4 for further description on method and values used in the calculations. Lines at the top of the figure compare the best estimates and uncertainty ranges (5 to 95% confidence range) with RF estimates from AR4.

Therefore, the large uncertainty in the aerosol forcing is the main cause of the large uncertainty in the total anthropogenic ERF. The total anthropogenic forcing is *virtually certain* to be positive with the probability for a negative value less than 0.1%. Compared to AR4 the total anthropogenic ERF is more strongly positive with an increase of 43%. This is caused by a combination of growth in GHG concentration, and thus strengthening in forcing of WMGHG, and weaker ERF estimates of aerosols (aerosol–radiation and aerosol–cloud interactions) as a result of new assessments of these effects.

Figure 8.17 shows the forcing over the Industrial Era by emitted compounds (see Supplementary Material Tables 8.SM.6 and 8.SM.7 for actual numbers and references). It is more complex to view the RF by emitted species than by change in atmospheric abundance (Figure 8.15) since the number of emitted compounds and changes leading to RF is larger than the number of compounds causing RF directly (see Section 8.3.3). The main reason for this is the indirect effect of several compounds and in particular components involved in atmospheric chemistry (see Section 8.2). To estimate the RF by the emitted compounds in some cases the emission over the entire Industrial Era is needed (e.g., for CO₂) whereas for other compounds (such as ozone and CH₄) quite complex simulations are required (see Section 8.3.3). CO₂ is the dominant positive forcing both by abundance and by emitted compound. Emissions of CH₄, CO, and NMVOC all lead to excess CO₂ as one end product if the carbon is of fossil origin and is the reason why the RF of direct CO₂ emissions is slightly lower than the RF of abundance change of CO₂. For CH₄ the contribution from emission is estimated to be almost twice as large as that from the CH₄ concen-

tration change, 0.97 (0.80 to 1.14) W m^{-2} versus 0.48 (0.43 to 0.53) W m^{-2} , respectively. This is because emission of CH_4 leads to ozone production, stratospheric water vapour, CO_2 (as mentioned above), and importantly affects its own lifetime (Section 8.2). Actually, emissions of CH_4 would lead to a stronger RF via the direct CH_4 greenhouse effect (0.64 W m^{-2}) than the RF from abundance change of CH_4 (0.48 W m^{-2}). This is because other compounds have influenced the lifetime of CH_4 and reduced the abundance of CH_4 , most notably NO_x . Emissions of CO (0.23 (0.18 to 0.29) W m^{-2}) and NMVOC (0.10 (0.06 to 0.14) W m^{-2}) have only indirect effects on RF through ozone production, CH_4 and CO_2 and thus contribute an overall positive RF. Emissions of NO_x , on the other hand, have indirect effects that lead to positive RF through ozone production and also effects that lead to negative RF through

reduction of CH_4 lifetime and thus its concentration, and through contributions to nitrate aerosol formation. The best estimate of the overall effect of anthropogenic emissions of NO_x is a negative RF (-0.15 (-0.34 to $+0.02$) W m^{-2}). Emissions of ammonia also contribute to nitrate aerosol formation, with a small offset due to compensating changes in sulphate aerosols. Additionally indirect effects from sulphate on atmospheric compounds are not included here as models typically simulate a small effect, but there are large relative differences in the response between models. Impacts of emissions other than CO_2 on the carbon cycle via changes in atmospheric composition (ozone or aerosols) are also not shown owing to the limited amount of available information.

For the WMGHG, the ERF best estimate is the same as the RF. The uncertainty range is slightly larger, however. The total emission-based ERF of WMGHG is 3.00 (2.22 to 3.78) W m^{-2} . That of CO_2 is 1.68 (1.33 to 2.03) W m^{-2} ; that of CH_4 is 0.97 (0.74 to 1.20) W m^{-2} ; that of stratospheric ozone-depleting halocarbons is 0.18 (0.01 to 0.35) W m^{-2} .

Emissions of BC have a positive RF through aerosol–radiation interactions and BC on snow (0.64 W m^{-2} , see Section 8.3.4 and Section 7.5). The emissions from the various compounds are co-emitted; this is in particular the case for BC and OC from biomass burning aerosols. The net RF of biomass burning emissions for aerosol–radiation interactions is close to zero, but with rather strong positive RF from BC and negative RF from OC (see Sections 8.3.4 and 7.5). The ERF due to aerosol–cloud interactions is caused by primary anthropogenic emissions of BC, OC and dust as well as secondary aerosol from anthropogenic emissions of SO_2 , NO_x and NH_3 . However, quantification of the contribution from the various components to the ERF due to aerosol–cloud interactions has not been attempted in this assessment.

8.5.2 Time Evolution of Historical Forcing

The time evolution of global mean forcing is shown in Figure 8.18 for the Industrial Era. Over all time periods during the Industrial Era CO_2 and other WMGHG have been the dominant term, except for shorter periods with strong volcanic eruptions. The time evolution shows an almost continuous increase in the magnitude of anthropogenic ERF. This is the case both for CO_2 and other WMGHGs as well as several individual aerosol components. The forcing from CO_2 and other WMGHGs has increased somewhat faster since the 1960s. Emissions of CO_2 have made the largest contribution to the increased anthropogenic forcing in every decade since the 1960s. The total aerosol ERF (aerosol–radiation interaction and aerosol–cloud interaction) has the strongest negative forcing (except for brief periods with large volcanic forcing), with a strengthening in the magnitude similar to many of the other anthropogenic forcing mechanisms with time. The global mean forcing of aerosol–radiation interactions was rather weak until 1950 but strengthened in the latter half of the last century and in particular in the period between 1950 and 1980. The RF due to aerosol–radiation interaction by aerosol component is shown in Section 8.3.4 (Figure 8.8).

Although there is *high confidence* for a substantial enhancement in the negative aerosol forcing in the period 1950–1980, there is much more uncertainty in the relative change in global mean aerosol forcing over the last two decades (1990–2010). Over the last two decades there has been a strong geographic shift in aerosol and aerosol precursor

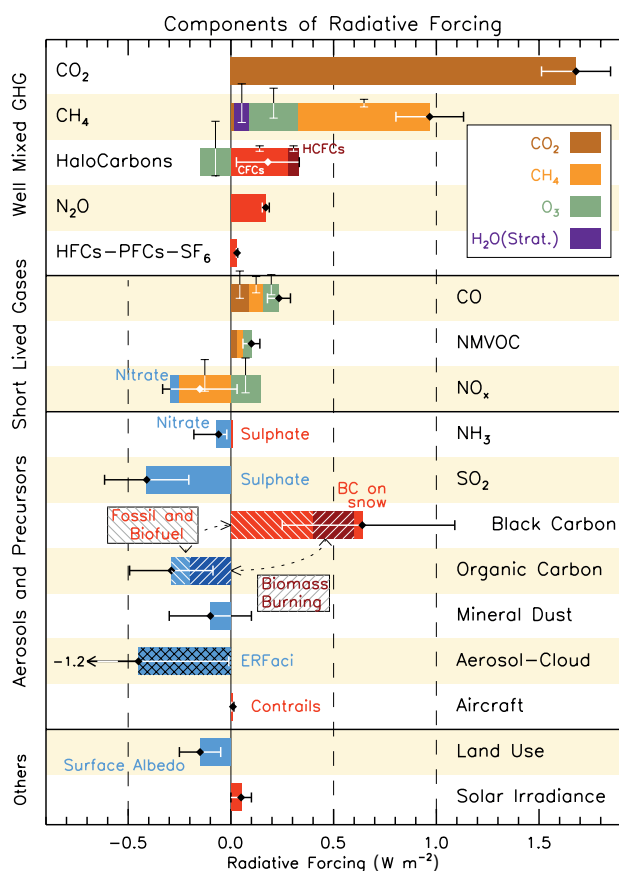


Figure 8.17 | RF bar chart for the period 1750–2011 based on emitted compounds (gases, aerosols or aerosol precursors) or other changes. Numerical values and their uncertainties are shown in Supplementary Material Tables 8.SM.6 and 8.SM.7. Note that a certain part of CH_4 attribution is not straightforward and discussed further in Section 8.3.3. Red (positive RF) and blue (negative forcing) are used for emitted components which affect few forcing agents, whereas for emitted components affecting many compounds several colours are used as indicated in the inset at the upper part of the figure. The vertical bars indicate the relative uncertainty of the RF induced by each component. Their length is proportional to the thickness of the bar, that is, the full length is equal to the bar thickness for a $\pm 50\%$ uncertainty. The net impact of the individual contributions is shown by a diamond symbol and its uncertainty (5 to 95% confidence range) is given by the horizontal error bar. ERFaci is ERF due to aerosol–cloud interaction. BC and OC are co-emitted, especially for biomass burning emissions (given as Biomass Burning in the figure) and to a large extent also for fossil and biofuel emissions (given as Fossil and Biofuel in the figure where biofuel refers to solid biomass fuels). SOA have not been included because the formation depends on a variety of factors not currently sufficiently quantified.

emissions (see Section 2.2.3), and there are some uncertainties in these emissions (Granier et al., 2011). In addition to the regional changes in the aerosol forcing there is also likely a competition between various aerosol effects. Emission data indicate a small increase in the BC emissions (Granier et al., 2011) but model studies also indicate a weak enhancement of other aerosol types. Therefore, the net aerosol forcing depends on the balance between absorbing and scattering aerosols for aerosol–radiation interaction as well as balance between the changes in aerosol–radiation and aerosol–cloud interactions. In the ACCMIP models, for example, the RF due to aerosol–radiation interaction becomes less negative during 1980 to 2000, but total aerosol ERF becomes more negative (Shindell et al., 2013c). There is a *very low confidence* for the trend in the total aerosol forcing during the past two to three decades, even the sign; however, there is *high confidence* that the offset from aerosol forcing to WMGHG forcing during this period was much smaller than over the 1950–1980 period.

The volcanic RF has a very irregular temporal pattern and for certain years has a strongly negative RF. There has not been a major volcanic eruption in the past decade, but some weaker eruptions give a current RF that is slightly negative relative to 1750 and slightly stronger in magnitude compared to 1999–2002 (see Section 8.4.2).

Figure 8.19 shows linear trends in forcing (anthropogenic, natural and total) over four different time periods. Three of the periods are the same as chosen in Box 9.2 (1984–1998, 1998–2011 and 1951–2011) and the period 1970–2011 is shown in Box 13.1. Monte Carlo simulations are performed to derive uncertainties in the forcing based on ranges given in Table 8.6 and the derived linear trends. Further, these uncertainties are combined with uncertainties derived from shifting time periods ± 2 years and the full 90% confidence range is shown in Figure 8.19 (in Box 9.2 only the total forcing is shown with uncertainties derived from the forcing uncertainty without sensitivity to time period). For the anthropogenic forcing sensitivity to the selection of time periods is very small with a maximum contribution to the uncertainties shown in Figure 8.19 of 2%. However, for the natural forcing the sensitivity to time periods is the dominant contributor to the overall uncertainty (see Supplementary Material Figure 8.SM.3) for the relatively short periods 1998–2011 and 1984–1998, whereas this is not the case for the longer periods. For the 1998–2011 period the natural forcing is *very likely* negative and has offset 2 to 89% of the anthropogenic forcing. It is *likely* that the natural forcing change has offset at least 30% of the anthropogenic forcing increase and *very likely* that it has offset at least 10% of the anthropogenic increase. For the 1998–2011 period both the volcanic and solar forcings contribute to this negative natural forcing, with the latter dominating. For the other periods shown in Figure 8.19 the best estimate of the natural is much smaller in magnitude than the anthropogenic forcing, but note that the natural forcing is very dependent on the selection of time period near the 1984–1998 interval. Over the period 1951–2011 the trend in anthropogenic forcing is almost 0.3 W m^{-2} per decade and thus anthropogenic forcing over this period is more than 1.5 W m^{-2} . The anthropogenic forcing for 1998–2011 is 30% higher and with smaller uncertainty than for the 1951–2011 period. Note that due to large WMGHG forcing (Section 8.3.2) the anthropogenic forcing was similar in the late 1970s and early 1980s to the 1998–2011 period. The reason for the reduced uncertainty in the 1998–2011 anthropogenic forcing

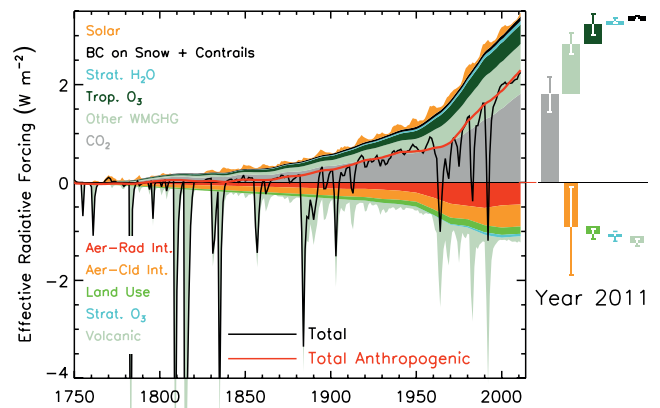


Figure 8.18 | Time evolution of forcing for anthropogenic and natural forcing mechanisms. Bars with the forcing and uncertainty ranges (5 to 95% confidence range) at present are given in the right part of the figure. For aerosol the ERF due to aerosol–radiation interaction and total aerosol ERF are shown. The uncertainty ranges are for present (2011 versus 1750) and are given in Table 8.6. For aerosols, only the uncertainty in the total aerosol ERF is given. For several of the forcing agents the relative uncertainty may be larger for certain time periods compared to present. See Supplementary Material Table 8.SM.8 for further information on the forcing time evolutions. Forcing numbers provided in Annex II. The total anthropogenic forcing was 0.57 (0.29 to 0.85) W m^{-2} in 1950, 1.25 (0.64 to 1.86) W m^{-2} in 1980 and 2.29 (1.13 to 3.33) W m^{-2} in 2011.

is the larger domination of WMGHG forcing and smaller contribution from aerosol forcing compared to previous periods. Similar to the results for 1970–2011 in Figure 8.19, Box 13.1 shows that the global energy budget is dominated by anthropogenic forcing compared to the natural forcing, except for the two major volcanic eruption in this period as can be easily seen in Figure 8.18.

Figure 8.20 shows the forcing between 1980 and 2011. Compared to the whole Industrial Era the dominance of the CO_2 is larger for this recent period both with respect to other WMGHG and the total anthropogenic RF. The forcing due to aerosols is rather weak leading

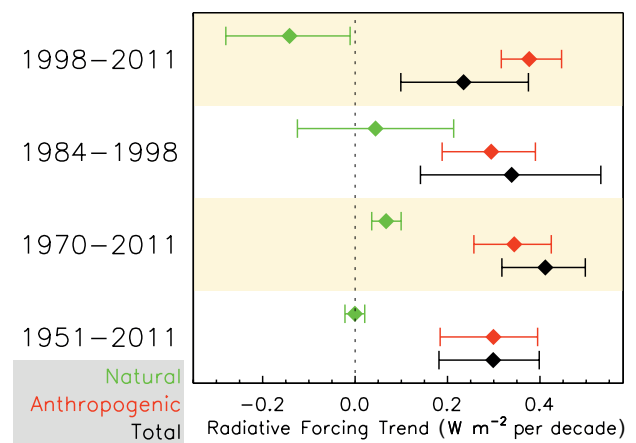


Figure 8.19 | Linear trend in anthropogenic, natural and total forcing for the indicated time periods. The uncertainty ranges (5 to 95% confidence range) are combined from uncertainties in the forcing values (from Table 8.6) and the uncertainties in selection of time period. Monte Carlo simulations were performed to derive uncertainties in the forcing based on ranges given in Table 8.6 and linear trends in forcing. The sensitivity to time periods has been derived from changing the time periods by ± 2 years.

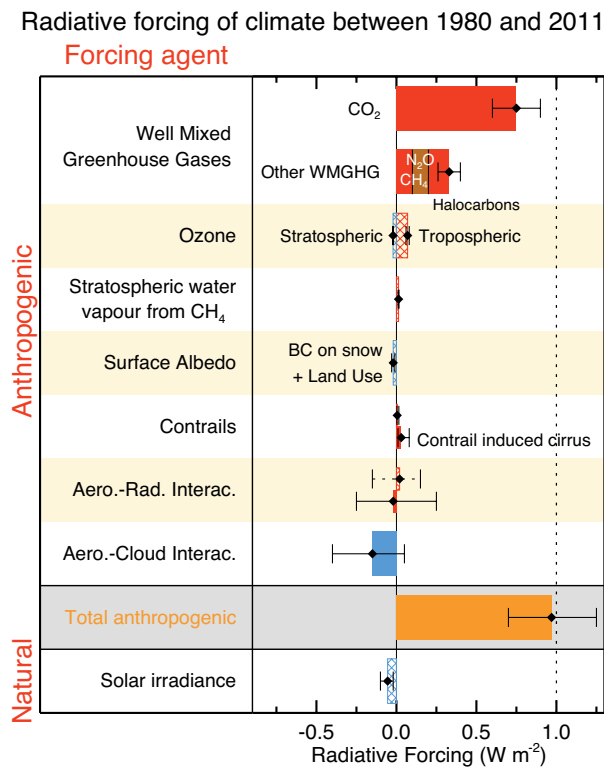


Figure 8.20 | Bar chart for RF (hatched) and ERF (solid) for the period 1980–2011, where the total anthropogenic ERF are derived from Monte-Carlo simulations similar to Figure 8.16. Uncertainties (5 to 95% confidence range) are given for RF (dotted lines) and ERF (solid lines).

to a very strong net positive ERF for the 1980–2011 period. More than 40% of the total anthropogenic ERF has occurred over the 1980–2011 period with a value close to 1.0 (0.7 to 1.3) W m^{-2} . The major contribution to the uncertainties in the time evolution of the anthropogenic forcing is associated with the aerosols (see Section 8.5.1). Despite this, anthropogenic ERF is *very likely* considerably more positive than the natural RF over the decadal time periods since 1950. This is in particular the case after 1980, where satellite data are available that provide important measurements to constrain the natural RF mechanisms (e.g., the volcanic RF change between 2007–2011 and 1978–1982 is 0.06 W m^{-2} and the representative change in solar irradiance over the 1980–2011 period is -0.06 W m^{-2}) with total natural RF of 0.0 (-0.1 to $+0.1$) W m^{-2} .

8.5.3 Future Radiative Forcing

Projections of global mean RF are assessed based on results from multiple sources examining the RF due to RCP emissions: the ACCMIP initiative (see Section 8.2) provides analysis of the RF or ERF due to aerosols and ozone (Shindell et al., 2013c), while WMGHG, land use and stratospheric water RFs are taken from the results of calculations with the reduced-complexity Model for the Assessment of Greenhouse-gas Induced Climate Change 6 (MAGICC6) driven by the RCP emissions and land use (Meinshausen et al., 2011a). While MAGICC6 also estimated ozone and aerosol RF, those values differ substantially from the ACCMIP values and are considered less realistic. Additional discussion of biases in the MAGICC6 results due to the simplified representations

of atmospheric chemistry and the carbon cycle, along with further discussion on the representativeness of the RCP projections in context with the broader set of scenarios in the literature, is presented in Section 11.3.5 and Section 12.3 (also see Section 8.2). As the ACCMIP project provided projected forcings primarily at 2030 and 2100, we hereafter highlight those times. Although understanding the relative contributions of various processes to the overall effect of aerosols on forcing is useful, we emphasize the total aerosol ERF, which includes all aerosol–radiation and aerosol–cloud interactions, as this is the most indicative of the aerosol forcing driving climate change. We also present traditional RF due to aerosol–radiation interaction (previously called direct aerosol effect) but do not examine further the various components of aerosol ERF. Aerosol forcing estimates, both mean and uncertainty ranges, are derived from the 10 ACCMIP models, 8 of which are also CMIP5 models. We analyze forcing during the 21st century (relative to 2000), and hence the WMGHG forcing changes are in addition to persistent forcing from historical WMGHG increases.

Analysis of forcing at 2030 relative to 2000 shows that under RCP2.6, total ozone (tropospheric and stratospheric) forcing is near zero, RF due to aerosol–radiation interaction is positive but small, and hence WMGHG forcing dominates changes over this time period (Figure 8.21). WMGHG forcing is dominated by increasing CO_2 , as declining CH_4 and increasing N_2O have nearly offsetting small contributions to forcing. Aerosol ERF was not evaluated for this RCP under ACCMIP, and values cannot be readily inferred from RF due to aerosol–radiation interaction as these are not directly proportional. Under RCP8.5, RF due to aerosol–radiation interaction in 2030 is weakly negative, aerosol ERF is positive with a fairly small value and large uncertainty range, total ozone forcing is positive but small ($\sim 0.1 \text{ W m}^{-2}$), and thus WMGHG forcing again dominates with a value exceeding 1 W m^{-2} . As with RCP2.6, WMGHG forcing is dominated by CO_2 , but under this scenario the other WMGHGs all contribute additional positive forcing. Going to 2100, ozone forcing diverges in sign between the two scenarios, consistent with changes in the tropospheric ozone burden (Figure 8.4) which are largely attributable to projected CH_4 emissions, but is small in either case. Ozone RF is the net impact of a positive forcing from stratospheric ozone recovery owing to reductions in anthropogenic ozone-depleting halocarbon emissions in both scenarios and a larger impact from changes in tropospheric precursors (Shindell et al., 2013c) which have a negative forcing in RCP2.6 and a positive forcing in RCP8.5.

The two scenarios are fairly consistent in their trends in RF due to aerosol–radiation interaction by component (Figure 8.21). There is positive RF due to aerosol–radiation interaction due to reductions in sulfate aerosol. This is largely offset by negative RF due to aerosol–radiation interaction by primary carbonaceous aerosols and especially by nitrate (though nearly all CMIP5 models did not include nitrate), leaving net aerosol RF due to aerosol–radiation interaction values that are very small, 0.1 W m^{-2} or less in magnitude, in either scenario at 2030 and 2100. Nitrate aerosols continue to increase through 2100 as ammonia emissions rise steadily due to increased use of agricultural fertilizer even as all other aerosol precursor emissions decrease (Figure 8.2), including sulphur dioxide which drives the reduction in sulphate aerosol that also contributes to additional formation of nitrate aerosols in the future (Bauer et al., 2007; Bellouin et al., 2011). Aerosol ERF is *likely* similar at this time in all scenarios given that they all have greatly

reduced emissions of all aerosols and aerosol precursors other than ammonia. Aerosol ERF shows a large positive value at 2100 relative to 2000, nearly returning to its 1850 levels (the 2100 versus 1850 ERF represents a decrease in ERF of 91% relative to the 2000 versus 1850 value), as is expected given the RCP emissions. Thus although some models project large increases in nitrate RF in the future, the reduction in overall aerosol loading appears to lead to such a strong reduction in aerosol ERF that the impact of aerosols becomes very small under these RCPs. Of course the projections of drastic reductions in primary aerosol as well as aerosol and ozone precursor emissions may be overly optimistic as they assume virtually all nations in the world become wealthy and that emissions reductions are directly dependent on wealth. The RCPs also contain substantially lower projected growth in HFC emissions than in some studies (e.g., Velders et al., 2009).

Although aerosol ERF becomes less negative by nearly 1 W m^{-2} from 2000 to 2100, this change is still small compared with the increased WMGHG forcing under RCP8.5, which is roughly 6 W m^{-2} during this time (Figure 8.21). Roughly 5 W m^{-2} of this WMGHG forcing comes from CO_2 , with substantial additional forcing from increases in both CH_4 and nitrous oxide and only a very small negative forcing from reductions in halocarbons. Under RCP2.6, the WMGHG forcing is only about 0.5 W m^{-2} during this time, as relatively strong decreases in CH_4 and halocarbon forcing offset roughly 40% of the increased CO_2 forcing, which is itself far less than under RCP8.5. Hence under this scenario, the projected future forcing due to aerosol reductions is actually stronger than the WMGHG forcing. Viewing the timeseries of the various forcings, however, indicates that aerosol ERF is returning to its pre-industrial levels, so that net forcing becomes increasingly dominated by WMGHGs regardless of scenario during the 21st century (Figure 8.22). As the forcing is so heavily dominated by WMGHGs at 2100, and the WMGHG concentrations (CO_2) or emissions (others) were chosen to match forcing targets, all the scenarios show net forcing values at that time that are fairly close to the scenarios' target values. The reduced aerosol forcing, with its large uncertainty, leads to a pronounced decrease in the uncertainty of the total net forcing by 2100. Based on the spread across ACCMIP models (using ERF for aerosols and converting to ERF for GHGs), the 90% confidence interval (CI) is about 20% for the 2100 net forcing, versus 26% for 2030 under RCP8.5 and 45–61% for 1980 and 2000 (Shindell et al., 2013c). The total ERF due to all causes has been independently estimated based on the transient response in the CMIP5 models and a linear forcing-response relationship derived through regression of the modelled response to an instantaneous increase in CO_2 (Forster et al., 2013). Uncertainties based on model spread behave similarly, with the 90% CI for net total ERF decreasing from 53% for 2003 to only 24 to 34% for 2100. Forcing relative to 2000 due to land use (via albedo only) and stratospheric water vapor changes are not shown separately as their projected values under the four RCPs are quite small: -0.09 to 0.00 and -0.03 to 0.10 W m^{-2} , respectively.

The CMIP5 forcing estimates (Forster et al., 2013) for the total projected 2030 and 2100 ERF are slightly smaller than the results obtained from the ACCMIP models (or the RCP targets; see Section 12.3.3). Examining the subset of models included in both this regression analysis and in ACCMIP shows that the ACCMIP subset show forcings on the low side of the mean value obtained from the full set of CMIP5

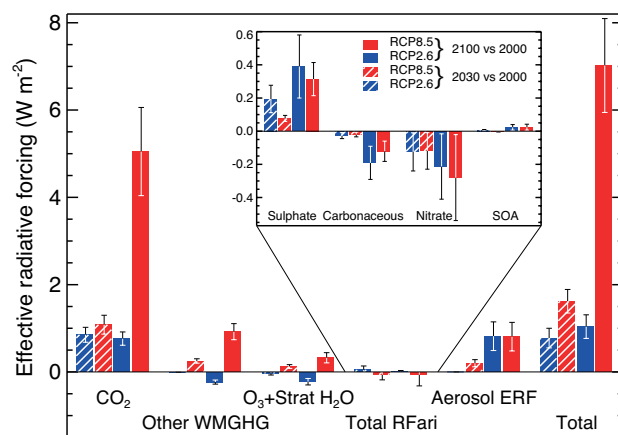


Figure 8.21 | Radiative forcing relative to 2000 due to anthropogenic composition changes based on ACCMIP models for aerosols (with aerosol ERF scaled to match the best estimate of present-day forcing) and total ozone and RCP WMGHG forcings. Ranges are one standard deviation in the ACCMIP models and assessed relative uncertainty for WMGHGs and stratospheric water vapor. Carbonaceous aerosols refer to primary carbonaceous, while SOA are secondary organic aerosols. Note that 2030 ERF for RCP2.6 was not available, and hence the total shown for that scenario is not perfectly comparable to the other total values. RFari is RF due to aerosol–radiation interaction.

analyzed, indicating that the discrepancy between the methods is not related to analysis of a different set of models. Instead, it may reflect nonlinearities in the response to forcing that are not represented by the regression analysis of the response to abrupt CO_2 increase experiments (Long and Collins, 2013) or differences in the response to other forcing agents relative to the response to CO_2 used in deriving the CMIP5 estimates (see also 12.3.3).

Natural forcings will also change in the future. The magnitudes cannot be reliably projected, but are likely to be small at multi-decadal scales (see Section 8.4). Brief episodic volcanic forcing could be large, however.

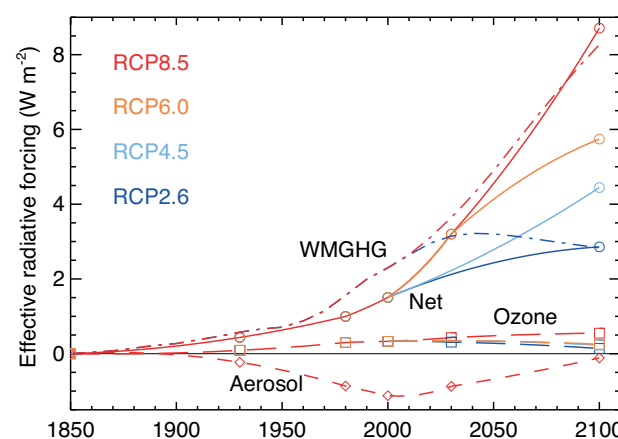


Figure 8.22 | Global mean anthropogenic forcing with symbols indicating the times at which ACCMIP simulations were performed (solid lines with circles are net; long dashes with squares are ozone; short dashes with diamonds are aerosol; dash-dot are WMGHG; colours indicate the RCPs with red for RCP8.5, orange RCP6.0, light blue RCP4.5, and dark blue RCP2.6). RCPs 2.6, 4.5 and 6.0 net forcings at 2100 are approximate values using aerosol ERF projected for RCP8.5 (modified from Shindell et al., 2013c). Some individual components are omitted for some RCPs for visual clarity.